Available online at www.sciencedirect.com
ScienceDirect
Journal of Solid State Chemistry 180 (2007) 2044–2052
JOURNAL OF SOLID STATE CHEMISTRY
www.elsevier.com/locate/jssc

A large series of isotypic Mo(V) diphosphates with a tunnel structure: From $A(MoO)_{10}(P_2O_7)_8$ with A = Ba, Sr, Ca, Cd, Pb to $A(MoO)_5(P_2O_7)_4$ with A = Ag, Li, Na, K

André Leclaire*, Vincent Caignaert, Bernard Raveau

Laboratoire CRISMAT-ENSICAEN, UMR CNRS 6508, 6 boulevard du maréchal Juin, 14050 CAEN cedex, France

Received 14 February 2007; received in revised form 11 May 2007; accepted 14 May 2007
Available online 18 May 2007

Abstract

The single crystal structure of a series of nine isotypic Mo(V) diphosphates was determined from crystals with composition $A^{2+}(MoO)_{10}(P_2O_7)_8$ (A = Ba, Sr, Ca, Cd, Pb) and $A^{+}(MoO)_5(P_2O_7)_4$ (A = Ag, Li, Na, K). The structure of those phosphates, built up of corner sharing MoO_6 octahedra, MoO_5 tetragonal pyramids and P_2O_7 diphosphates groups, forms eight-sided tunnels as described by Lii et al. for A = Ag. New features are evidenced: (1) existence of two orientations, up and down along b for the MoO_5 pyramids; (2) maximum insertion rate of the divalent cations which is twice less than that of the univalent cations; (3) different behavior of the series "Pb, Sr, Ba, Li, Na, K" which exhibits only one kind of site for the inserted cation, compared to the "Cd, Ca, Ag" series for which two kinds of sites are observed; (4) off-centering of the A-site cations with respect to the tunnel axis; and (5) unusually high thermal factors along the tunnel axis, but absence of ionic conductivity.

Keywords: Molybdenum(V) phosphates; Molybdenum(V) diphosphates; Three-dimensional frameworks; Tunnel structures

1. Introduction

Numerous phosphates of pentavalent molybdenum have been synthesized after the discovery of the first Mo(V) phosphate $MoPO_5$ by Kierkegaard and Westerlund [1]. One remarkable feature of these compounds deals with the particular geometry of the MoO_6 octahedra which are always isolated, i.e., only linked to PO_4 tetrahedra and exhibit one free corner, leading to one abnormally short molybdenyl Mo═O bond (for a review see Ref [2]).

Among the various Mo(V) phosphates, the diphosphate $Ag(MoO)_5(P_2O_7)_4$, discovered by Lii et al. [3] is of great interest from the structural view point. These authors observed that, in this tunnel structure, the silver cations exhibit large thermal factors along the direction of the tunnels, suggesting positional disorder and consequently possible ionic conductivity. Moreover, they could obtain isotypic phases for lithium and sodium, but did not solve their structure due to the too small size of the crystals. Interestingly, they detected the existence of a similar structure for polycrystalline powders of composition $AMo_5P_8O_{33}$ with A = Ca, Sr, Ba, Pb, but they noticed the presence of unindexed reflections and a small amount of MoO_2. Bearing in mind these results, we have revisited the systems A–Mo^{5+}–P–O.

Single crystals of nine phosphates could be grown to a suitable size. Their crystal structure determination shows that they all exhibit the same framework $[Mo_5P_8O_{33}]\infty$ as $Ag(MoO)_5(P_2O_7)_4$, described by Lii et al. [3], but evidences two different formula, depending on the valency of the inserted cation, i.e., $A(MoO)_5(P_2O_7)_4$ for univalent cations A = Li, Na, Ag, K and $A(MoO)_{10}(P_2O_7)_8$ for divalent cations A = Ba, Sr, Ca, Cd, Pb. Importantly, we observe that the A cations exhibit unusually high thermal factors along the direction of the tunnel, i.e., U_{22} values up to 0.46 Å^2, but our complexe impedance measurements show the absence of ionic conductivity, in agreement with the rather large distance between two successive A sites along that direction.

*Corresponding author. Fax: +33 2 31 95 16 00.
E-mail address: andre.leclaire@ensicaen.fr (A. Leclaire).

0022-4596/$ - see front matter © 2007 Elsevier Inc. All rights reserved.
doi:10.1016/j.jssc.2007.05.004

1.1. Single crystal growth

The largest single crystals were obtained for the lead phosphate $Pb(MoO)_{10}(P_2O_7)_8$ from a batch of nominal composition $Pb_2Br_2Mo_2P_4O_{17}$. First PbO, $H(NH_4)_2PO_4$ and MoO_3 were mixed in an agate mortar in the molar ratio 1:8:4, and heated at 673 K in a platinum crucible to decompose the ammonium phosphate. All the precursors were of analytical grade purity and were used as supplied by Prolabo, Merck or Aldrich without further purifications. In a second step, the resulting mixture added to PbO and $PbBr_2$ (1:1) was crushed in an agate mortar and sealed in an evacuated quartz ampoule and then heated for 1 day at 873 K, cooled at 2 K/h to 473 K and finally quenched to room temperature.

From the greenish sintered product, some well-formed green crystals of very good quality were extracted. The EDS analysis of those crystals is consistent with the ratio 1:10:16 for the Pb, Mo, and P elements. The quality of those crystals is better than that previously obtained for the silver phosphate, allowing more reliable results to be obtained.

The quantitative synthesis of $Pb(MoO)_{10}(P_2O_7)_8$ in the form of polycrystalline green powder was carried out using process similar to the previous one. First, a mixture of $H(NH_4)_2PO_4$ and MoO_3 with molar ratio 16:8.333 was heated in air at 673 K. The resulting mixture was added to molybdenum powder and PbO (1.666:1), sealed in an evacuated quartz ampoule, heated for 24 h at 923 K and finally cooled in the same way as for the crystal growth.

For the Ca, Sr, and Ba compounds green crystals were obtained from batches of nominal composition $A^{2+}Mo_{10}P_{16}O_{66}$ using a two-steps process. First, a mixture of ACO_3, $H(NH_4)_2PO_4$ and MoO_3 with molar ratio 1:16:8.333 was heated in air at 673 K. Then the resulting product was added to molybdenum powder (1.666 mole), crushed, sealed in an evacuated quartz ampoule, heated at 1073 K during 24 h and cooled as previously described.

The Cd compound single crystals were obtained in a similar way from a batch of nominal composition $CdMo_4P_6O_{26}$.

For A = Li, Na, K, and Ag, the crystals were grown from $AMo_5P_8O_{33}$ batches with the same process as the divalent cations but using nitrate for the Ag isotype instead of carbonates for the alkaline ions.

1.2. Crystal structure determinations

The data of the nine studied compounds were recorded at room temperature on a NONIUS KAPPA CCD diffractometer using the MoKα radiation ($\lambda = 0.71073$ Å) isolated with a graphite monochromator. The lattice parameters reported in Table 1 were refined from the complete data sets, which show a "m" Laue symmetry. The systematic absences $h+k = 2n+1$ in the whole space and $l = 2n+1$ and $h = 2n+1$ in $h0l$, and $k = 2n+1$ in $0k0$ are consistent with the Cc (9) and $C2/c$ (15) space groups. The Patterson function maps show the $u0w$ and $u\frac{1}{2}w$ Harker peaks characteristic of the centro-symmetrical $C2/c$ space group.

The structure of $Pb(MoO)_{10}(P_2O_7)_8$ was solved by the heavy atom method and refined using a full matrix least-squares method performed on the F_{hkl} values weighted by $1/\sigma(F)^2$ (JANA2000 package [4]).

For the eight other compounds, the atomic coordinates of the lead phosphate were used as starting hypothesis and subsequent differences in Fourier maps allowed the coordinates of the cations to be found and in some cases, to observe a splitting of the pyramidal molybdenum sites and of the free apex of the MoO_5 pyramid over two neighbor sites. Measurement and refinement parameters and crystal data are summarized in Table 1. Further details of the crystals structure investigations can be obtained

Table 1
Crystal parameters and refinement data

	$PbMo_{10}P_{16}O_{66}$	$CdMo_{10}P_{16}O_{66}$	$CaMo_{10}P_{16}O_{66}$	$SrMo_{10}P_{16}O_{66}$	$BaMo_{10}P_{16}O_{66}$	$AgMo_5P_8O_{33}$	$LiMo_5P_8O_{33}$	$NaMo_5P_8O_{33}$	$KMo_5P_8O_{33}$
a (Å)	32.4685	32.3785	32.4246	32.4147	32.4154	32.4977	31.9893	32.3526	32.5473
b (Å)	4.8460	4.8487	4.8404	4.8325	4.8323	4.8490	4.8501	4.8449	4.8333
c (Å)	23.0118	22.9057	22.9466	22.9034	23.0185	22.9957	22.7489	22.9068	23.0637
α (deg)	90.0	90.0	90.0	90.0	90.0	90.0	90.0	90.0	90.0
β (deg)	134.469	134.848	134.921	134.517	134.330	134.779	134.170	134.658	134.587
γ (deg)	90.0	90.0	90.0	90.0	90.0	90.0	90.0	90.0	90.0
V (Å^3)	2583.9	2549.5	2550.1	2558.2	2579.2	2572.2	2531.6	2554.0	2584.3
Density	3.4925	3.416	3.321	3.372	3.409	3.519	3.311	3.324	3.327
μL mm^{-1}	6.239	3.443	3.137	4.058	3.750	3.750	3.058	3.049	3.158
T_{min}	0.3611	0.8655	0.7718	0.8430	0.8583	0.8560	0.8377	0.9109	0.7053
T_{max}	0.8189	0.9642	0.9417	0.9330	0.9607	0.9633	0.9546	0.9550	0.9641
Crystal size (μm)	34 × 36 × 364	11 × 14 × 72	20 × 24 × 160	18 × 20 × 70	14 × 14 × 68	12 × 14 × 76	16 × 18 × 106	16 × 18 × 80	12 × 16 × 250
N_{hkl}	8946	5092	7366	5297	4380	5252	5336	5428	5344
$N_{hkl\ observed}$	5936	2809	3305	2479	1315	2757	3279	3093	2514
$N_{b.\ param.}$	241	225	222	219	139	231	222	222	219
R	0.0358	0.0585	0.0465	0.0611	0.0658	0.0507	0.0443	0.0541	0.0567
R_w	0.0296	0.0487	0.0400	0.0554	0.0546	0.0425	0.0415	0.0494	0.0481

from the Fachinformationszentrum Karlsruhe, 76344 Eggenstein-Leopoldshafen, Germany (fax: +(49)-7247-808-666; e-mail: crysdata@fiz.karlsruhe.de) on quoting the depository numbers CSD 417722 for Ag, CSD 417723 for Ba, CSD 417724 for Ca, CSD 417725 for Cd, CSD 417726 for K, CSD 417727 for Li, CSD 417728 for Na, CSD 417729 for Pb, and CSD 417730 for Sr.

1.3. Description of the host lattice $[Mo_5P_8O_{33}]\infty$

The framework $[Mo_5P_8O_{33}]\infty$ is very similar for all the member of the series. The projection of this structure for $Pb(MoO)_{10}(P_2O_7)_8$ along *b* (Fig. 1) shows that this framework is, as expected, close to that previously described by Lii et al. [3] for $Ag(MoO)_5(P_2O_7)_4$. In agreement with these authors, one observes that the structure consists of three sorts of polyhedra: MoO_6 octahedra, MoO_5 pyramids, and diphosphate groups P_2O_7. All these polyhedra share corners to built up a framework, which delimits large eight-sided tunnels containing lead and empty elongated tunnels, running along *b*. As in numerous molybdenum phosphates containing P_2O_7 groups, one diphosphate unit shares two corners with the same octahedron (Mo1 or Mo2) leading to the well-known MoP_2O_{11} unit (Fig. 2). As a consequence, the $[Mo_5P_8O_{33}]\infty$ framework consists of $[MoP_2O_{10}]\infty$ ladder-like columns running along *b* (Fig. 3), where the MoO_6 octahedra play the role of steps. Four columns share corners to form a $[Mo_4P_8O_{32}]\infty$ tube parallel to *b* (Fig. 1). The so-formed tubes are connected through MoO_5 square pyramids (Mo3) leading to the $[Mo_5P_8O_{33}]\infty$ frameworks.

One particular feature of this structure concerns the orientation of the MoO_5 square pyramids which are found to form rows along *b*, with their apical oxygen pointing always in the same direction, so that they can form strongly elongated octahedra (Fig. 4a). More importantly, two orientations (up and down) are possible for such pyramids from one row to the other (Fig. 4b). They correspond to the splitting of the molybdenum site on both sides of the square basis of the pyramid, and involve the appearance of an additional site for the apical oxygen. Remarkably, one indeed observes these additional sites Mo4 and *O*13b, for all the compounds that we have investigated except for Pb. Nevertheless, the occupancy factor of Mo4 is by far not equal to that of Mo3 and varies significantly with the nature of the *A*-site cation. The Mo4 site is almost empty for Li, i.e., of 0.03, whereas an occupancy factor ranging from 0.1 to 0.16 is observed for Sr, K, Ba, and Na, and higher factors of 0.17, 0.26, and 0.50 are found for Ag, Cd, and Ca, respectively. Note that such a phenomenon was not observed by Lii et al. [3] for $Ag(MoO)_5(P_2O_7)_4$. This difference may be explained by the fact that these authors could not collect enough data to obtain low *R* factors. But another possibility deals with the fact that such a

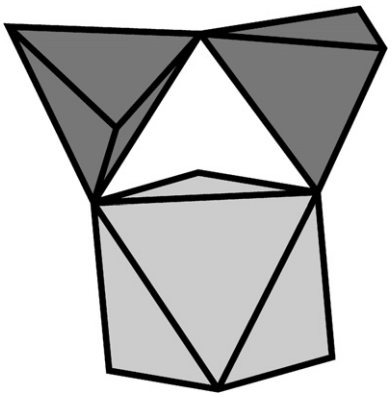

Fig. 2. The MoP_2O_{11} unit with the P_2O_7 diphosphate group sharing two corners with the same MoO_6 octahedron.

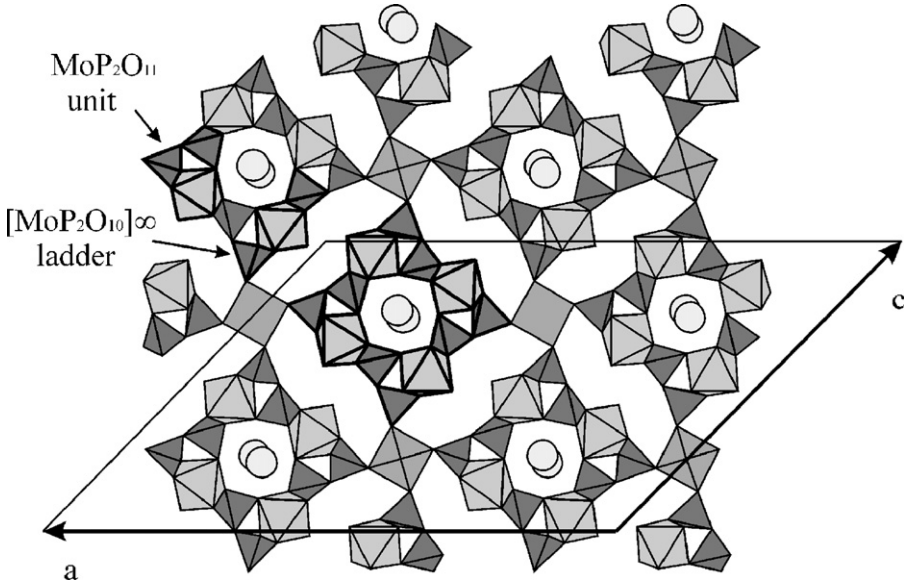

Fig. 1. The projection of the structure of $Pb(MoO)_{10}(P_2O_7)_8$ along the *b*-axis.

distribution of Mo between two sites may be closely related to the experimental conditions of synthesis.

For the nine frameworks, the geometry of the MoO_6 octahedra, Mo1 and Mo2, is very similar (Table 2), characteristic of that observed in all Mo(V) phosphates.

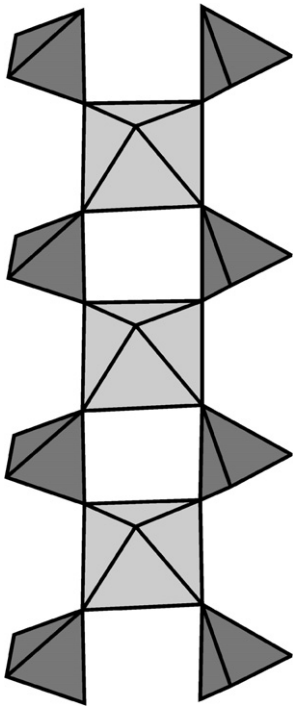

Fig. 3. The $[MoP_2O_{10}]\infty$ ladder-like column running along the *b*-axis.

One indeed observes a very short bond molybdenyl bond (1.621(5)–1.675(13) Å) opposed to a very long one (2.214(6)–2.239(5) Å) and four medium bonds (1.989(4)–2.047(8) Å).

As discussed above, the existence of a square pyramidal coordination for Mo(V) in phosphates is rather rare. Nevertheless, it corresponds to a strongly elongated octahedron, characterized by a short molybdenyl bond (1.668(5)–1.691(3) Å) opposed to an extremely long Mo–O bond (>2.90 Å), and four medium ones (1.957(8)–2.047(7) Å).

The interatomic distances in the PO_4 tetrahedra (Table 3) show that the geometry of the P_2O_7 groups is similar to that usually observed with longer P–O distances (1.567(7)–1.615 Å) for the bridging oxygen, and P–O distances ranging from 1.458(11) to 1.542(11)Å, for the other atoms.

1.4. The particular behavior of the A-site cations

As mentioned above, the A cations sit in the eight-sided tunnels, leaving the elongated tunnels empty. The first important feature concerns the insertion rate, which is twice less for the divalent cations than for the univalent cations, in spite of the large number of available sites. This demonstrates that the stability of such a structure clearly requires the only presence of Mo(V), due to the particular geometry of its MoO_6 octahedra and MoO_5 pyramids. These results also explain why Lii et al. [3] did not succeed to prepare $A(MoO)_5(P_2O_7)_4$ phosphates as pure phases for

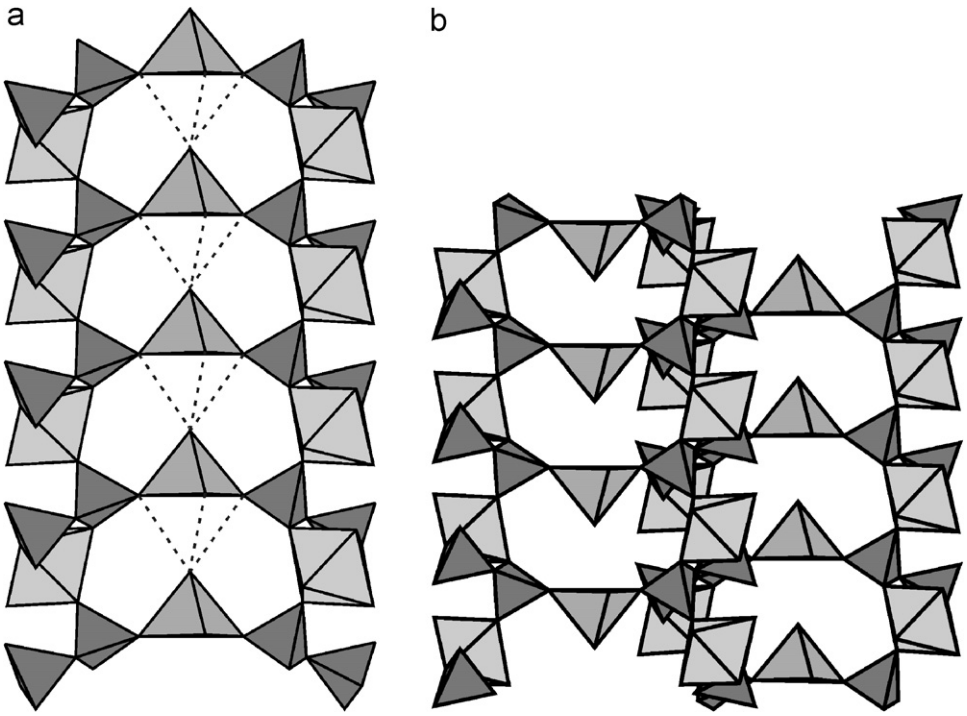

Fig. 4. (a) The stacking of the MoO_5 pyramids along *b*, leading to a chain of elongated MoO_6 octahedra. (b) The two orientations of the MoO_5 pyramids in the $Mo_5P_8O_{33}$ frameworks.

A divalent cations, which would correspond to mixed valent Mo(IV)–Mo(V) phosphates.

The second interesting feature deals with the types of sites available in the structure and their occupancy factors. Two different kinds of behavior are observed. For the series "Pb, Sr, Ba, Li, Na, K", only one type of sites (Fig. 5a) is occupied by these cations, with an occupancy factor of 50% for univalent cations and of 25% for

Table 2
The molybdenum–oxygen distances (Å) in the MoO_6 octahedra and in the MoO_5 pyramids

	$PbMo_{10}P_{16}O_{66}$	$CdMo_{10}P_{16}O_{66}$	$CaMo_{10}P_{16}O_{66}$	$SrMo_{10}P_{16}O_{66}$	$BaMo_{10}P_{16}O_{66}$	$AgMo_5P_8O_{33}$	$LiMo_5P_8O_{33}$	$NaMo_5P_8O_{33}$	$KMo_5P_8O_{33}$
Mo(1)–O(1)	1.644(2)	1.627(5)	1.650(5)	1.615(5)	1.656(6)	1.644(5)	1.630(5)	1.626(5)	1.621(5)
Mo(1)–O(2)	2.009(3)	2.016(7)	1.999(4)	2.001(7)	2.001(9)	2.005(6)	1.995(4)	1.997(7)	2.012(7)
Mo(1)–O(3)	2.026(2)	2.021(5)	2.028(3)	2.019(5)	2.027(7)	2.018(3)	2.031(3)	2.023(5)	2.024(5)
Mo(1)–O(4)	2.023(3)	2.007(8)	2.013(5)	2.021(8)	2.003(12)	2019(6)	2.027(5)	2.018(8)	2.017(8)
Mo(1)–O(5)	2.034(2)	2.024(6)	2.039(4)	2.011(6)	2.076(7)	2.046(4)	2.038(4)	2.036(5)	2.029(6)
Mo(1)–O(6)	2.232(2)	2.239(5)	2.235(3)	2.222(5)	2.209(8)	2.226(5)	2.233(3)	2.232(5)	2.235(5)
Mo(2)–O(7)	1.649(3)	1.635(7)	1.632(6)	1.634(8)	1.675(13)	1.639(7)	1.646(5)	1.649(7)	1.646(7)
Mo(2)–O(8)	2.006(2)	2.017(5)	2.004(3)	2.016(5)	2.014(6)	2.009(4)	1.989(4)	1.994(4)	2.019(4)
Mo(2)–O(9)	2.024(2)	2.003(4)	2.011(2)	2.023(4)	2.023(5)	2.023(4)	2.002(3)	2.012(4)	2.020(4)
Mo(2)–O(10)	2.032(2)	2.024(5)	2.026(3)	2.027(6)	2.047(8)	2.032(5)	2.021(5)	2.036(5)	2.036(5)
Mo(2)–O(11)	2.035(3)	2.026(7)	2.020(4)	2.015(7)	2.015(10)	2.033(6)	2.036(6)	2.037(7)	2.032(7)
Mo(2)–O(12)	2.228(3)	2.233(7)	2.224(5)	2.215(7)	2.224(10)	2.223(6)	2.223(5)	2.214(6)	2.227(3)
Mo(3)–O(13a)	1.691(3)	1.669(2)	1.668(2)	1.668(2)	1.668(2)	1.669(2)	1.669(1)	1.669(2)	1.669(2)
Mo(3)–O(14)	1.975(3)	1.977(8)	1.991(5)	1.974(8)	1.943(12)	1.986(7)	1.970(5)	1.974(8)	1.977(7)
Mo(3)–O(14^{i})	1.975(3)	1.977(8)	1.991(5)	1.974(8)	1.943(12)	1.986(7)	1.970(5)	1.974(8)	1.977(7)
Mo(3)–O(15)	1.981(1)	1.983(4)	1.962(2)	1.974(4)	1.996(6)	1.981(3)	1.986(2)	1.982(3)	1.987(3)
Mo(3)–O(15^{i})	1.981(1)	1.983(4)	1.962(2)	1.974(4)	1.996(6)	1.981(3)	1.986(2)	1.982(3)	1.987(3)
Occupancy Mo(3)	1.000	0.742(1)	0.5490(8)	0.908(1)	0.844(1)	0.8312(8)	0.9711(7)	0.8369(9)	0.891(1)
Mo(4)–O(13b)		1.668(4)	1.668(2)	1.667(14)	1.667(14)	1.668(6)	1.668(30)	1.668(5)	1.667(7)
Mo(4)–O(14)		1.962(8)	1.962(5)	1.964(9)	1.968(12)	1.956(7)	1.993(8)	1.957(8)	1.979(7)
Mo(4)–O(14^{i})		1.962(8)	1.962(5)	1.964(9)	1.968(12)	1.956(7)	1.993(8)	1.957(8)	1.979(7)
Mo(4)–O(15)		2.012(4)	1.992(2)	2.015(5)	2.034(7)	2.003(3)	2.047(7)	2.019(3)	2.008(3)
Mo(4)–O(15^{i})		2.012(4)	1.992(2)	2.015(5)	2.034(7)	2.003(3)	2.047(7)	2.019(3)	2.008(3)
Occupancy Mo(4)	0.0	0.258(1)	0.4510(8)	0.092(1)	0.156(1)	0.1688(8)	0.0289(7)	0.1637(9)	0.109(1)

Table 3
The phosphorus–oxygen bond lengths in the P_2O_7 diphosphate units

	$PbMo_{10}P_{16}O_{66}$	$CdMo_{10}P_{16}O_{66}$	$CaMo_{10}P_{16}O_{66}$	$SrMo_{10}P_{16}O_{66}$	$BaMo_{10}P_{16}O_{66}$	$AgMo_5P_8O_{33}$	$LiMo_5P_8O_{33}$	$NaMo_5P_8O_{33}$	$KMo_5P_8O_{33}$
P(1)–O(9^{ii})	1.507(2)	1.525(5)	1.524(3)	1.501(5)	1.520(7)	1.518(5)	1.507(4)	1.513(5)	1.513(5)
P(1)–O(10)	1.511(2)	1.501(4)	1.504(3)	1.499(5)	1.476(6)	1.501(4)	1.496(3)	1.490(4)	1.499(4)
P(1)–O(14)	1.521(2)	1.524(7)	1.520(4)	1.534(7)	1.542(11)	1.517(7)	1.519(4)	1.525(7)	1.509(7)
P(1)–O(16)	1.586(3)	1.578(7)	1.580(5)	1.570(7)	1.603(10)	1.590(6)	1.581(5)	1.569(7)	1.572(7)
P(2)–O(2^{iii})	1.505(2)	1.484(5)	1.505(3)	1.508(5)	1.514(6)	1.504(4)	1.507(3)	1.504(4)	1.501(4)
P(2)–O(3)	1.523(3)	1.534(7)	1.523(6)	1.513(7)	1.542(11)	1.533(6)	1.524(4)	1.525(7)	1.512(7)
P(2)–O(12)	1.507(1)	1.515(4)	1.501(3)	1.498(4)	1.517(6)	1.507(3)	1.506(3)	1.506(3)	1.507(4)
P(2)–O(16)	1.601(3)	1.600(8)	1.597(5)	1.599(8)	1.608(12)	1.595(7)	1.599(5)	1.601(8)	1.592(8)
P(1)–P(2)	2.857(1)	2.875(4)	2.862(2)	2.847(4)	2.845(7)	2.867(3)	2.860(3)	2.855(3)	2.836(3)
P(1)–O(16)–P(2)	127.4(1)	129.6(3)	128.5(1)	127.9(3)	124.7(4)	128.4(2)	128.1(1)	128.5(3)	127.4(3)
P(3)–O(4)	1.514(2)	1.518(5)	1.522(3)	1.501(5)	1.516(7)	1.506(4)	1.510(3)	1.509(5)	1.515(5)
P(3)–O(5^{iii})	1.509(3)	1.511(8)	1.496(4)	1.519(8)	1.458(11)	1.501(7)	1.493(5)	1.501(7)	1.503(8)
P(3)–O(15^{iv})	1.519(2)	1.515(7)	1.521(4)	1.500(7)	1.521(12)	1.510(5)	1.514(5)	1.505(5)	1.514(5)
P(3)–O(17)	1.587(2)	1.582(6)	1.580(3)	1.578(6)	1.585(9)	1.587(6)	1.585(3)	1.585(6)	1.572(6)
P(4)–O(6^{iii})	1.505(3)	1.498(9)	1.496(5)	1.507(9)	1.504(13)	1.511(8)	1.483(5)	1.509(9)	1.498(9)
P(4)–O(8^{v})	1.505(3)	1.470(7)	1.494(4)	1.486(7)	1.471(10)	1.493(6)	1.497(7)	1.494(7)	1.484(7)
P(4)–O(11^{vi})	1.523(2)	1.534(5)	1.517(3)	1.537(5)	1.524(6)	1.530(4)	1.502(4)	1.520(4)	1.518(4)
P(4)–O(17)	1.601(2)	1.587(5)	1.600(3)	1.593(5)	1.595(7)	1.598(3)	1.587(3)	1.591(5)	1.615(4)
P(3)–P(4)	2.8683(6)	2.877(2)	2.869(1)	2.864(2)	2.860(3)	2.873(2)	2.869(1)	2.869(2)	2.851(2)
P(3)–O(17)–P(4)	128.3(2)	130.5(6)	128.8(3)	129.1(6)	128.2(8)	128.8(5)	129.5(4)	129.2(6)	126.9(5)

Codes——i: $-x, y, \frac{1}{2}-z$; ii : $x, 1+y, z$; iii: $x, y-1, z$; iv: $x, 1-y, z-\frac{1}{2}$; v: $\frac{1}{2}-x, y-\frac{1}{2}, \frac{1}{2}-z$; vi: $\frac{1}{2}-x, \frac{1}{2}+y, \frac{1}{2}-z$; vii: $\frac{1}{2}-x, \frac{1}{2}-y, z-\frac{1}{2}$.

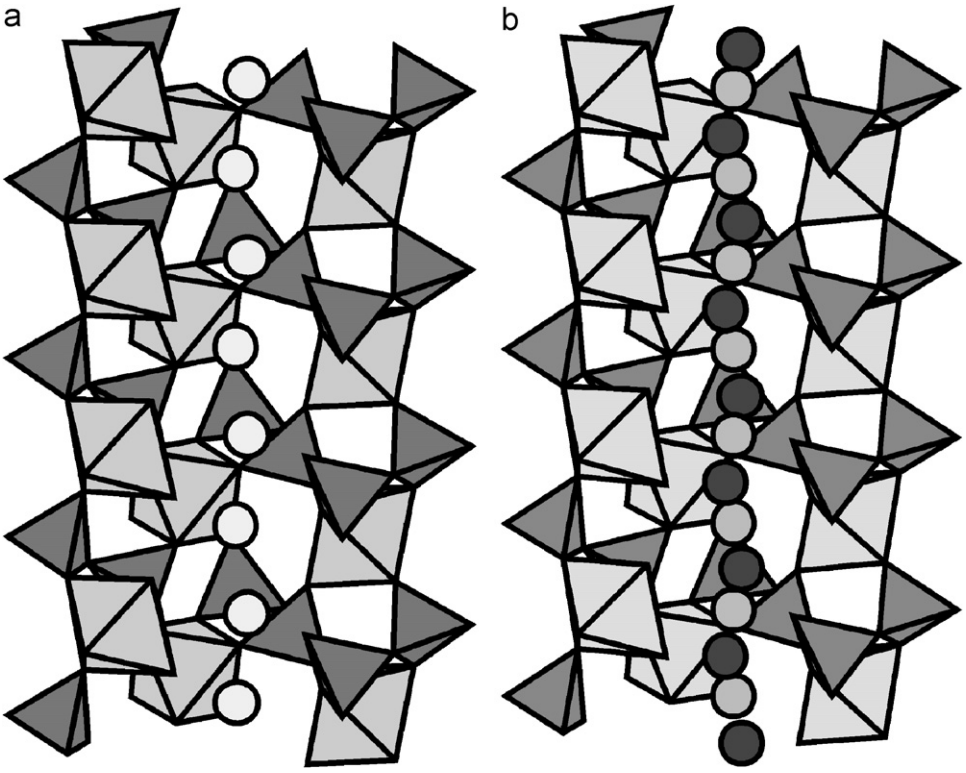

Fig. 5. (a) The setting of Pb, Sr, Ba, Li, Na, or K in the tunnels running along *b*. (b) The two sitting available for Cd, Ca, and Ag.

Table 4
The cations–oxygen distances in the tunnels

	Pb	Cd(1)^{vi}	Cd(2)	Ca(1)^{vii}	Ca(2)^{vii}	Sr^{v}	Ba	Ag(1)^{vi}	Ag(2)	Li^{vi}	Na^{vi}	K
O(3)	*2.451(2)*	*2.370(7)*	2.979(7)	2.792(9)	**2.270(8)**	**2.440(6)**	2.537(6)	*2.422(7)*	2.96(1)	2.32(3)	*2.41(1)*	*2.515(5)*
O(3)^{v}			2.633(7)	2.876(8)			3.226(7)		2.75(1)			
O(6)	2.597(3)	2.696(9)			2.676(9)	2.592(9)	2.588(8)	2.78(1)		*2.18(3)*	2.70(2)	2.617(9)
O(6)^{iii}			2.753(8)	2.811(8)					2.79(1)			
O(6)^{v}	2.619(2)	2.487(7)	**2.297(8)**	2.379(8)	2.540(7)	2.579(7)	2.654(6)	2.503(6)	**2.359(9)**	3.05(4)	2.48(1)	2.609(7)
O(11)^{ii}	2.674(2)	2.88(1)			2.84(1)	2.63(1)	*2.50(1)*	2.88(1)			2.80(2)	2.64(1)
O(11)^{vi}	3.029(4)	2.72(1)	*2.37(1)*	**2.31(1)**	2.83(1)	3.05(1)	3.34(1)	2.76(1)	*2.39(1)*	2.41(4)	2.78(2)	3.16(1)
O(12)	2.941(4)	2.82(1)	2.45(1)	*2.54(1)*	2.76(1)	2.91(1)	3.090(9)	2.82(1)	2.49(1)		2.83(2)	3.00(1)
O(12)^{ii}							3.186(9)					
O(12)^{vi}	**2.420(3)**	**2.27(1)**	2.83(1)	2.64(1)	*2.41(1)*	**2.44(1)**	**2.49(1)**	**2.35(1)**	2.84(2)	**2.03(4)**	**2.34(2)**	**2.46(1)**
Coord.	7	7	7	7	7	7	9	7	7	4	7	7

Bold values indicate the shortest distance for each cations.

divalent cations. For the series "Cd, Ca, Ag", two types of sites are available for the cations with the same coordination number (Table 4). Besides the first type of site, a second type of site is located at half-way along *b* between two successive type-I sites (Fig. 5b). Then, the occupancy factors of both sites are 25% for Ag and 12.5% for Ca and Cd. The maximum occupancy factor of these sites is governed by the short distances between two successive sites along *b*, which implies that only one site out of two can be occupied by the cations in the series "Pb, Sr, Ba, Li, Na, K", whereas only one site out of four can be occupied for the series "Cd, Ca, Ag". No correlation seems to exist between the size of these cations, or their electronic configuration and the different behavior of these two series. In contrast, it is quite remarkable that the series "Cd, Ca, Ag" which involves these two types of sites, exhibits the highest splitting rate between the Mo3 and Mo4 sites in the square pyramids, with occupancy factors of Mo4 site ranging from 0.17 to 0.50. Thus, correlations may exist between the orientation of the MoO_5 pyramids and the nature of the cations located in the tunnels.

The third point deals with the fact that the *A* cations are off-centered with respect to the tunnel axis. The plot of the minimum value of the cation–oxygen distance versus the distance of the cation from the tunnel axis (Fig. 6) shows three areas. First, the farthest one contains the Li cation

which sits at 0.75 Å from the axis, i.e., close to the walls of the tunnels. Second, the divalent ions are sitting at distances ranging from 0.23 to 0.30 Å from the tunnel axis, and third, the univalent ions, except lithium, are the nearest from the tunnel (less than 0.23 Å). But no correlation seems to exist between the cation–oxygen distances and the distance from the axis. The same remarks can be made with the plot of the ionic radii versus the distances from the tunnel axis (Fig. 7), which is very similar to the previous one. More interesting is the plot of the values of the component U_{22} of the anisotropic thermal factors of the cations divided by its occupancy factor versus the distances from the tunnel axis (Fig. 8). One observes the particular behavior of the lithium ions, as seen previously, but for all the other cations the U_{22}/occup values are strongly correlated to the distances of these ions from the tunnel axis ($R^2 = 0.81$).

The fourth remarkable feature concerns the unusually high thermal factors along the tunnel axis (Table 5). U_{22} values up to 0.46 $Å^2$ are indeed observed, i.e., more than 10 times larger than expected for A cations in a classical structure. Again, no correlation can be found between the size of the cations, or their electronic configuration and the U_{22} values, the largest thermal factors ranging from 0.21 to 0.46 $Å^2$ for Pb, Sr, Ag, Na, K. In agreement with Lii et al. [3], we can consider the possibility of ionic conductivity, at least for these five compounds. Nevertheless, one must bear in mind that such values correspond to maximum

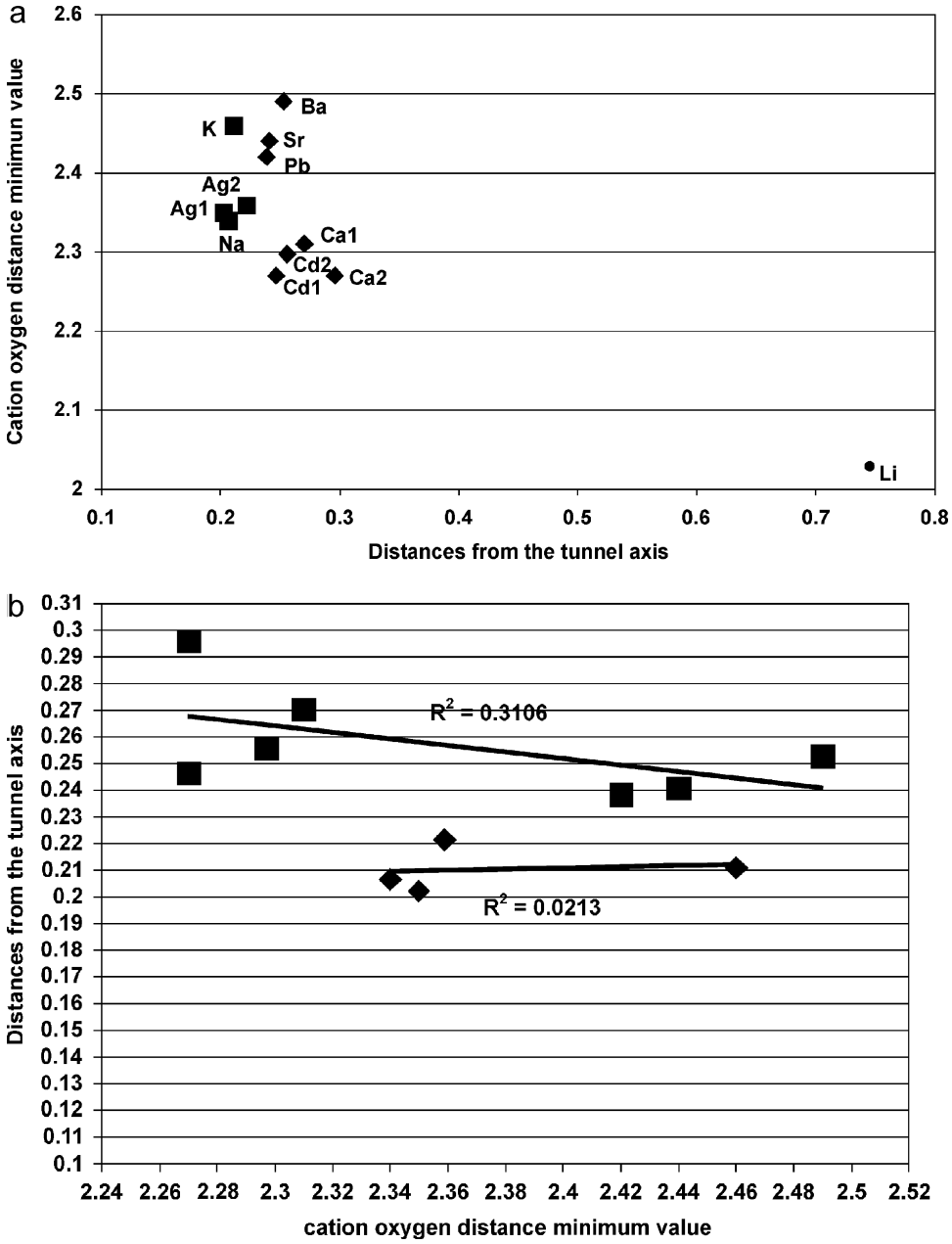

Fig. 6. The plot of the minimum values of the cation–oxygen distances in each polyhedron of coordination versus its distances from the axis of the tunnel.

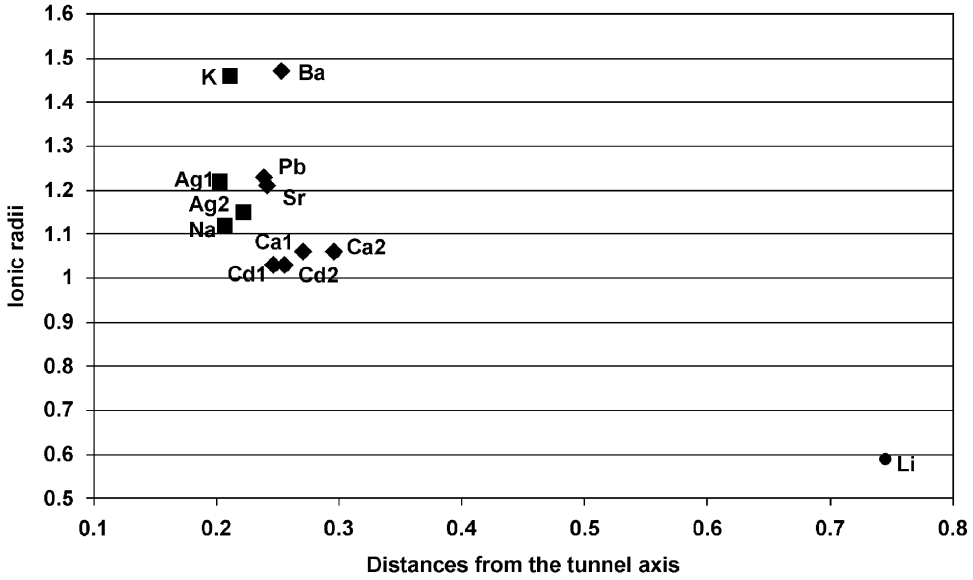

Fig. 7. The plot of the ionic radii of the cations versus its distances from the tunnel axis.

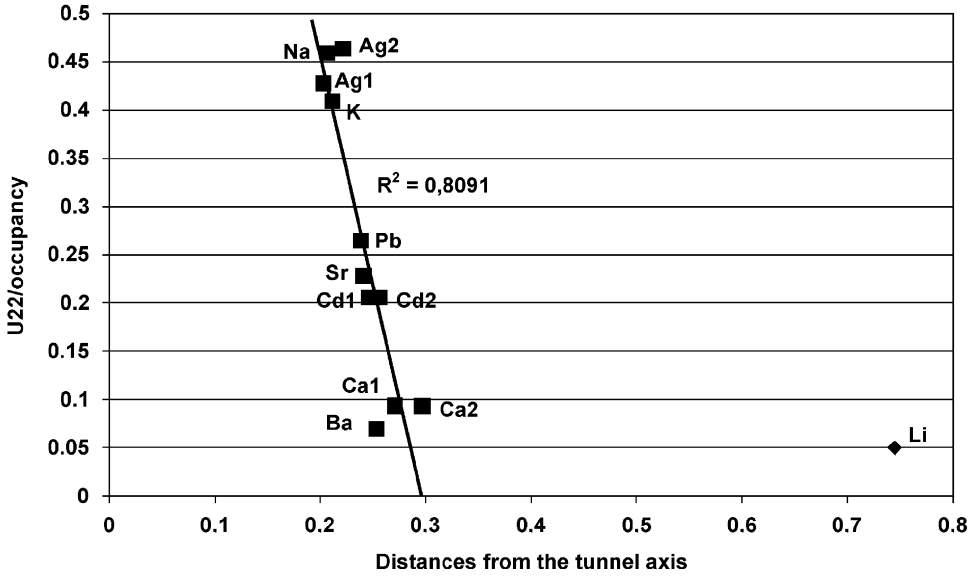

Fig. 8. The plot of the U_{22} component of the thermal motion of the cations divided by the cation occupancy versus the distances of the cations from the tunnel axis.

Table 5
The anisotropic thermal motion components in $A^{2+}(MoO)_{10}(P_2O_7)_8$ and in $A^{+}(MoO)_5(P_2O_7)_4$

	$PbMo_{10}P_{16}O_{66}$	$CdMo_{10}P_{16}O_{66}$	$CaMo_{10}P_{16}O_{66}$	$SrMo_{10}P_{16}O_{66}$	$BaMo_{10}P_{16}O_{66}$	$AgMo_5P_8O_{33}$	$LiMo_5P_8O_{33}$	$NaMo_5P_8O_{33}$	$KMo_5P_8O_{33}$
U11 A1	0.0127(2)	0.016(1)	0.011(2)	0.009(2)	0.014(1)	0.020(1)	0.04(1)	0.040(5)	0.005(2)
U22 A1	**0.265(3)**	**0.103(4)**	**0.047(2)**	**0.229(6)**	**0.070(2)**	**0.214(7)**	**0.05(1)**	**0.46(2)**	**0.41(1)**
U33 A1	0.0228(4)	0.021(2)	0.012(2)	0.024(2)	0.024(2)	0.022(2)	0.05(2)	0.024(5)	0.022(2)
U12 A1	−0.0046(8)	−0.007(3)	0.012(3)	−0.015(3)	0.006(1)	0.006(3)	−0.02(1)	0.093(9)	0.006(4)
U13 A1	0.0077(3)	0.013(1)	0.008(2)	0.007(2)	0.011(2)	0.015(1)	0.03(1)	0.021(5)	0.002(2)
U23 A1	0.0515(8)	−0.030(3)	0.006(2)	−0.062(3)	0.020(2)	−0.014(3)	−0.03(1)	0.030(9)	0.083(4)
Ueq A1	**0.105(1)**	**0.048(2)**	**0.023(3)**	**0.091(3)**	**0.040(2)**	**0.084(3)**	**0.05(2)**	**0.175(9)**	**0.153(5)**
U11 A2		0.016(1)	0.011(2)			0.027(2)			
U22 A2		**0.103(4)**	**0.047(2)**			**0.232(8)**			
U33 A2		0.021(2)	0.012(2)			0.024(2)			
U12 A2		−0.007(3)	0.012(3)			−0.027(4)			
U13 A2		0.013(1)	0.008(2)			0.019(2)			
U23 A2		−0.030(3)	0.006(2)			−0.034(3)			
Ueq A2		**0.048(2)**	**0.023(3)**			**0.093(3)**			

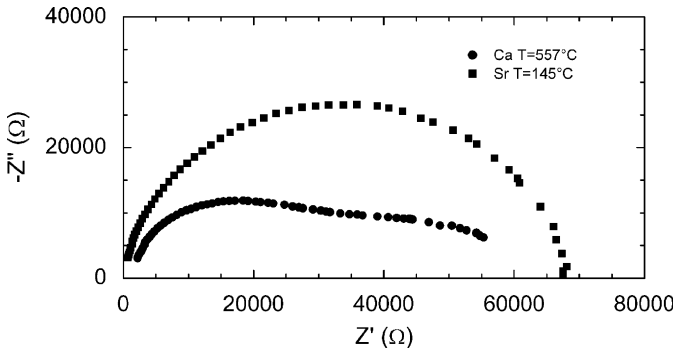

Fig. 9. Nyquist diagrams for $Ca(MoO)_{10}(P_2O_7)_8$ at 830 K and for $Sr(MoO)_{10}(P_2O_7)_8$ at 418 K.

displacements along *b*, ranging from about 0.5 Å for Pb, Sr, Ag to 0.7 Å for Na, K. Such values are significantly smaller than the distances between two successive sites, which are close to 2.4 Å for Pb, Sr, Na, K and 1.5 Å for Ag. In order to check the possibility of ionic conductivity, complex impedance measurements were carried out for several compounds.

Transport properties of samples were carried out by impedance spectroscopy using an EG&G 7220 lock-in amplifier in the frequency range 10–120 kHz with an ac signal amplitude of 10 mV. The measurements were made on sintered pellets with a diameter around 6 mm and thickness between 1 and 3 mm. Gold or platinum electrodes were deposited by vacuum evaporation. The impedance measurements were carried out at steady-state temperatures from room temperature to 900 K under an argon atmosphere.

Examples of the complexe impedance diagrams registered at different temperatures are given in Fig. 9 for Ca and Sr. Well-defined semicircular arcs passing through the origin at high frequencies, were observed. However one does not detect any upturn of Z'', followed by a linear evolution versus frequency, contrary to what should be obtained for classical electrolytes. These results clearly indicate that these materials cannot be considered as ionic conductors.

In conclusion, this study shows the great ability of the Mo(V) diphosphate framework "$Mo_5P_8O_{33}$" to accommodate various univalent and divalent cations, with a quite variable insertion rate ranging, from 1 to $\frac{1}{2}$, respectively. Thus, it appears that the stability of such a framework is before all dictated by the presence of Mo(V), which adopts the octahedral and pyramidal coordinations, both characterized by the well-known abnormally short molybdenyl bond. The ability of the MoO_5 pyramid to exhibit two different orientations—up and down—from one tunnel to the other is a remarkable feature of this structure. But the most important points deal with the quite variable occupancy of the two sites of the tunnels by *A* cations, the off-centering of the latter with respect to the tunnel axis and the high thermal factor of these cations along that direction. Nevertheless, it is worth pointing out that no ionic conductivity can be detected, likely due to the too large distance between two successive *A* sites along the tunnel axis. The possibility to intercalate or de-intercalate cations by soft chemistry methods in these materials will be investigated.

References

[1] P. Kierkegaard, M. Westerlund, Acta Chem. Scand. 18 (1964) 2.
[2] G. Costentin, A. Leclaire, M.-M. Borel, A. Grandin, B. Raveau, Rev. Inorg. Chem. 13 (1993) 77.
[3] K.H. Lii, D.C. Johnston, D.P. Goshorn, R.C. Haushalter, J. Solid State Chem. 71 (1987) 131.
[4] V. Petricek, M. Dusek, L. Palatinus, Jana2000. Structure Determination Software Programs, Institute of Physics, Praha, Czech Republic, 2000.